phys. stat. sol. (b) **244**, No. 8, 2707–2729 (2007) / **DOI** 10.1002/pssb.200675620

Feature Article

Development of GaInNAsSb alloys: Growth, band structure, optical properties and applications

James S. Harris Jr.[*], **R. Kudrawiec**[**], **H. B. Yuen, S. R. Bank, H. P. Bae, M. A. Wistey, D. Jackrel, E. R. Pickett, T. Sarmiento, L. L. Goddard, V. Lordi,** and **T. Gugov**

Solid State and Photonics Laboratory, Stanford University, CIS-X 328, Via Ortega, Stanford, California 94305-4075, USA

Received 1 December 2006, revised 20 February 2007, accepted 28 February 2007
Published online 11 July 2007

PACS 42.55.Px, 73.21.Fg, 78.55.Cr, 78.67.–n, 81.15.Hi, 85.35.–p

In the past few years, GaInNAsSb has been found to be a potentially superior material to both GaInNAs and InGaAsP for communications wavelength laser applications. It has been observed that due to the surfactant role of antimony during epitaxy, higher quality material can be grown over the entire 1.2–1.6 μm range on GaAs substrates. In addition, it has been discovered that antimony in GaInNAsSb also works as a constituent that significantly modifies the valence band. These findings motivated a systematic study of GaInNAsSb alloys with widely varying compositions. Our recent progress in growth and materials development of GaInNAsSb alloys and our fabrication of 1.5–1.6 μm lasers are discussed in this paper. We review our recent studies of the conduction band offset in (Ga,In) (N,As,Sb)/GaAs quantum wells and discuss the growth challenges of GaInNAsSb alloys. Finally, we report record setting long wavelength edge emitting lasers and the first monolithic VCSELs operating at 1.5 μm based on GaInNAsSb QWs grown on GaAs. Successful development of GaInNAsSb alloys for lasers has led to a much broader range of potential applications for this material including: solar cells, electroabsorption modulators, saturable absorbers and far infrared optoelectronic devices and these are also briefly discussed in this paper.

1 Introduction

Recent progress in molecular beam epitaxy (MBE) has led to successful growth of alloys composed of distinctly different semiconductor materials, including GaN and GaAs [1, 2]. GaNAs alloys with small amounts of nitrogen (<5%), referred to as dilute nitrides, have garnered great interest for their non-traditional energy band behaviour compared to other alloy semiconductors, see Fig. 1. The most interesting and unusual feature of GaNAs alloys is a large bandgap reduction due to incorporation of N atoms (~150 meV per% of N). In 1996, Kondow et al. [3] recognized that introducing appropriate amounts of nitrogen and indium into GaAs would reduce the lattice mismatch sufficiently to extend the emission wavelength to the technologically important 1.3 μm regime. This idea was the strongest driving force to grow dilute nitrides, since it is well known that low cost, long wavelength, single mode vertical cavity surface-emitting lasers (VCSELs), which can be directly modulated, operated uncooled in ambient environments, and easily packaged and coupled to fibre, are an essential element for expansion of high-speed telecommunication systems to metro, local and fibre to the home networks [4–6]. GaInNAs-based

[*] Corresponding author: e-mail: harris@snow.stanford.edu, Phone: +1 650 723 4659, Fax: +1 650 723 659
[**] e-mail: kudrawiec@snow.stanford.edu, robert.kudrawiec@pwr.wroc.pl

lasers, with emission at 1.3 μm and low threshold current, were achieved quickly [1, 2, 4–6]. Growth of GaInNAs-based lasers emitting at 1.55 μm proved much more difficult, since it was usually observed that the incorporation of nitrogen deteriorates the optical properties due to ion damage [7, 8], non-radiative traps [9, 10], and/or phase separation [11, 12]. These issues became increasingly apparent when the indium and nitrogen concentrations in GaInNAs were increased to extend the wavelength to >1.4 μm. Despite the mentioned problems, GaInNAs lasers emitting at ~1.55 μm have been demonstrated by a few groups [13–17].

In 1999, Yang et al. [18] demonstrated that Sb could be used as a surfactant in GaInNAs growth. In addition, it was discovered that Sb acts as both a surfactant (which dramatically improves material/optical quality in dilute-nitrides) and constituent (which reduces the bandgap and modifies bandgap line-up in GaInNAs/GaAs quantum wells) [6, 18–20]. Promising GaInNAsSb edge-emitting lasers [21] and VCSELs [22] operating just below 1.5 μm were demonstrated quite quickly. A successful realization of ~1.5 μm lasers with the lowest threshold current has been achieved by using a GaInNAsSb/GaNAs quantum well (QW) as the active region [22]. More recently, room-temperature continuous wave operation at 1.55 μm [23, 24] and 1.59 μm [25, 26] has been demonstrated by using GaInNAsSb/GaNAs QW active regions on GaAs.

Thus the MBE growth of semiconductor lasers containing quinary alloys became a reality. However our familiar question: "*is this quinary alloy a prototype system that provides the ultimate opportunity for bandgap engineering and novel devices, or is a recipe for a disaster of poorly controlled and non-reproducible epitaxial growth?*" [6] remained unanswered. The aim of this work is to respond to this question, since useful application of quinary alloys in semiconductor structures has to be reproducible and reliable. The most important issue is to know *what benefits are achieved with quinary alloys vs. quaternary or ternary alloys and how well they can be controlled.* Moreover, it is important to know *how to predict the band structure and optical properties of quinary alloys, GaInNAsSb in this case.* Our recent progress in the growth of GaInNAsSb/GaAs QWs with various compositions and systematic investigations of the optical properties and band structure by electromodulation spectroscopy provide definitive answer to these questions.

This paper is organized as follows: Section 2 first provides some general remarks regarding the growth of dilute nitrides, followed by our discovery of a relatively relaxed, broad growth regime for the growth of GaInNAsSb alloys with widely varying compositions. A summary of our recent studies of the band structure for (Ga,In)(N,As,Sb)/GaAs QWs and step-like GaInNAsSb/GaNAs/GaAs QWs is given in Section 3. Optical properties of GaInNAsSb QWs and investigations of optimal annealing conditions are reviewed in Section 4. Section 5 describes application of GaInNAsSb alloys to low threshold high power edge emitting lasers, the first momolitic 1.5 μm VCSEL and the potential for GaInNAsSb alloys to address a much broader range of devices.

2 Growth and structural characterization

In order to investigate the surfactant and constituent effect of antimony in GaInNAsSb alloys, a systematic investigation of the growth of GaInNAsSb QWs under a broad range of growth conditions has been performed [27]. Structural properties of these samples were studied by high-resolution X-ray diffraction (HRXRD), secondary-ion mass spectrometry (SIMS) and transmission electron microscopy (TEM) and optical properties by photoluminescence (PL). In this section, first some general remarks on the growth of dilute nitrides are provided; followed by a detailed description of the growth of GaInNAsSb/GaAs QWs in a relatively broad, easily controlled growth regime with widely varying compositions. Some results on the growth and structural characterization of GaInNAsSb/GaNAs/GaAs QWs, which are the active part of 1.5–1.6 μm lasers, are presented at the end of this section.

2.1 General remarks on the growth of dilute nitrides

The primary technologies for growing dilute nitrides are MBE [4–6, 28–37] and metalorganic vapor phase epitaxy (MOVPE) [38–42]. In this work, we focus on GaInNAsSb alloys grown by MBE only.

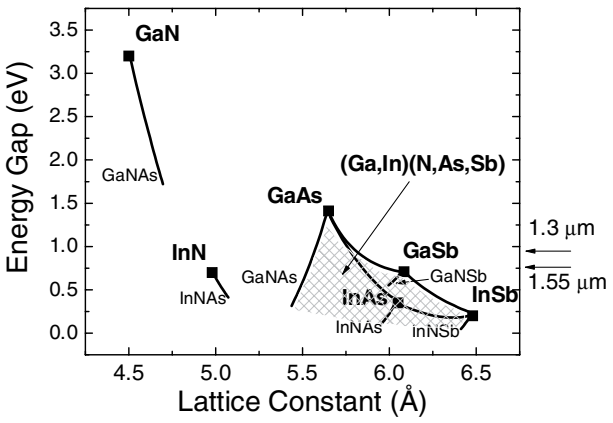

Fig. 1 Energy gap versus lattice constant for III–V compounds and dilute nitrides.

Due to the large mismatch (more than 20%) in the lattice constants of GaAs and GaN and large differences between As and N in their atomic orbital energies and sizes, the growth of GaNAs (and other dilute nitrides) is substantially different than all earlier III–V alloys [1, 2, 4–6, 43, 44]. It has been shown that GaNAs alloys are thermodynamically unstable since even infinitesimally small composition fluctuation decrease their free energy [45]. Similar behavior is expected after adding In and/or Sb atoms to GaNAs. Thus GaInNAsSb alloys are not stable, but metastable; they tend to separate rather than forming a homogeneous alloy, so the growth conditions must be carefully controlled to prevent this phase separation. In order to incorporate a sufficient amount of nitrogen into the material, the growth has to be done at much lower growth temperature than the growth of N-free alloys. This makes the growth window for dilute nitrides with sufficient N concentration quite narrow. This window becomes even narrower with increased indium content, since a tendency to three dimensional (3D) growth is stronger for GaInNAs with higher indium content. The main driving force to explore GaInNAsSb alloys was the observation that by incorporating Sb into GaInNAs, the growth window for good two dimensional (2D) epitaxy is not only expanded, but enables the incorporation of higher In and N compositions. It has also been observed that antimony concentration is much higher than dopant concentration, which is typical of reactive surfactants [46]. Sb is a group V element and therefore should be treated/considered in GaInNAs as a virtually-surfactant [46], which mediates in the epitaxy of GaInNAs and incorporates inside this alloy at a concentration much higher than typical dopant concentration. Under the optimum growth conditions, antimony is incorporated into the alloy at levels of 5–8%, well above the incorporation level of nitrogen. Hence, one is really forming a quinary alloy of GaInNAsSb. The growth of GaInNAsSb with antimony concentration above 1% becomes an interesting issue since it was expected that antimony, as a constituent, can significantly influence the bandgap line-up in GaInNAs/GaAs QWs. In addition, it is expected that the combination of GaInNAsSb alloys with new dilute nitrides (InNAs, GaNSb, and InNAsSb) will open way to grow new III–V structures for mid infra-red applications, as shown in Fig. 1.

One of most important and unexpected findings was that the atomic N sticking coefficient is near unity, i.e., the group III growth rate (*not* As flux) controls the N concentration when other growth parameters are held constant [47–49]. At substrate temperatures <500 °C, one does not need to control the As_2 flux, other than to keep the surface As stabilized. We grow with an As_2 overpressure that is 8–20 times the Ga pressure, much like the growth of GaAs or GaInAs. This is completely different than any other mixed column V, III–V alloy semiconductor system [50, 51]. This result is truly surprising and indicates that MBE growth of GaInNAs(Sb) should have major advantages in terms of yield and reproducibility as compared to InGaAsP [50–53]. Note that an influence of other growth parameters on the N incorporation was also observed [47, 54–56] but the control of N concentration (energy gap of GaInNAsSb) via group III rate seems to be the most reasonable from the practical/technological point of view.

Point defects, which are the origin of non-radiative recombination, are known to be one of the biggest problems for the dilute nitrides. Their concentration is higher than in N-free material grown under

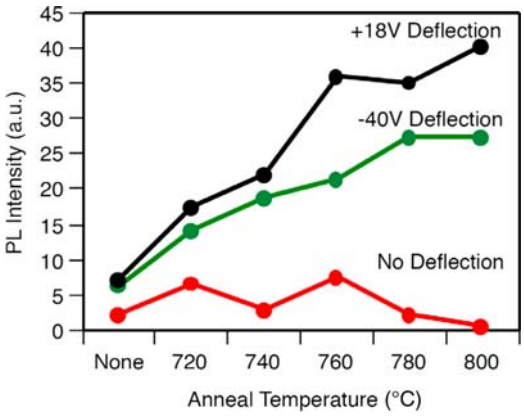

Fig. 2 (online colour at: www.pss-b.com) Photoluminescence for samples grown with different voltages applied to one deflection plate. The other plate was grounded. Note the higher photoluminescence over all annealing conditions [7].

optimal conditions because of the low growth temperature and requirement in MBE to use some type of plasma source to produce atomic nitrogen that is sufficiently reactive to be incorporated into the alloy. Another issue is the concentration of unintentional impurities. We have used SIMS to verify that the impurity concentration (H, O, C and B) is below 1×10^{17} cm^{-3} in our MBE-grown materials [48, 49]. It is very low compared to nitride-arsenides grown by gas source MBE or MOVPE because of the high purity of all the starting source elements. Thus, in our materials, the background impurities are less important than defects associated with the incorporation of nitrogen. In general, the nature of N-related defects is not well understood. A portion of these defects can usually be removed by post growth annealing. However, the first step to achieving high quality dilute nitrides is to reduce the number of N-related defects in as-grown materials. The N plasma source design and operation are major factors in N-related defect generation by ions from the plasma source. There are several approaches to reducing the numbers of ions from the output of a plasma source. The radio frequency (RF) power and gas flow rate have a strong effect on the fraction of ions in the output of the plasma source, with low RF power and high flow producing the fewest ions, but also the least atomic N. Similarly, we verified that using smaller, fewer holes in the aperture at the end of the plasma source decreased plasma damage and improved the stability of the plasma [57–59]. To remove the ions from the molecular beam, electrically biased metal plates were installed at the exit aperture of the nitrogen cell [6]. It has been found that this approach significantly improves the optical quality of GaInNAsSb QWs, as illustrated in Fig. 2. This discovery has been one of the keys to our successful realization of low threshold, long wavelength GaInNAsSb lasers, described in Section 4 of this paper.

2.2 Growth and structural characterization of GaInNAsSb quantum wells of widely varying compositions

To determine the effects and behavior of widely varying compositions on the structural, optical, and electronic properties of GaInNAsSb, several samples were grown at a variety of indium and antimony fluxes. The samples were grown on n-type (100) GaAs substrates by MBE in a Varian Mod. Gen-II system. Ga and In were supplied by SUMO effusion cells. A valved As cracker supplied As_2 and an unvalved Sb cracker supplied monomeric Sb. An arsenic overpressure of 2×10^{-7} Torr beam equivalent pressure (BEP) and an antimony flux of $2.0-10.0 \times 10^{-8}$ Torr BEP were supplied during the GaInNAsSb QW growth. N was supplied by a modified SVT Associates plasma cell operating at a RF of 13.56 MHz. N gas of 5N (99.999%) purity was filtered through a <1 part-per-billion Pall Mini-Gaskleen purifier to minimize oxygen contamination. The cell was operated with 300 W input power and a N gas flow of 0.5 sccm. As mentioned earlier, N incorporation into (In)GaAs is directly controlled by the group-III growth rate and obeys the equation

$$[\mathrm{N}\%] = \frac{K}{\{\mathrm{GR}\}}, \tag{1}$$

Table 1 A summary of the growth conditions for the samples described in this study. The intended indium composition and the applied antimony fluxes are listed. Series A denotes the series in which antimony was varied under constant "high" indium flux. Series B indicates the series in which antimony was varied under constant "low" indium flux. Series C illustrates the series in which indium was varied under constant 1.0×10^{-7} BEP torr antimony flux.

	8% In	16% In	24% In	32% In
0 Sb	B			A
2.0×10^{-8} BEP torr Sb	B			A
6.0×10^{-8} BEP torr Sb	B			A
1.0×10^{-7} BEP torr Sb	B, C	C	C	A, C

where [N%] is the percentage of nitrogen desired, K is a constant obtained from calibrations, and {GR} is the group-III growth rate in μm/h. The constant K is a function of nitrogen gas flow [60] into the RF plasma cell and the amount of antimony [61–63] present in the dilute-nitride layer.

A summary of the samples described below is shown in Table 1. The first series consisted of GaInNAs(Sb) QWs which were intended to contain 32% In and 2.0% N, a typical composition for 1.3 μm wavelength emission. These samples are considered to be in the "high In" and high lattice strain regime. The Sb flux was varied from zero to 1.0×10^{-7} torr BEP while all other growth parameters were held constant. 1.0×10^{-7} BEP torr is the typical flux we have used for all GaInNAsSb laser devices [64]. Next, a series of GaInNAs(Sb) QWs grown with much lower In, 8%, and 2.0% N were analyzed for their properties with varying amounts of Sb. These "low In" and low lattice strain regime samples correspond to the composition typically used to obtain 1.0 eV bandgap for solar cell applications. Finally a set of samples with constant 1.0×10^{-7} torr BEP Sb flux and varying In concentrations from the "low" to "high" In regimes were studied to connect the properties of the two previous series into a comprehensive understanding on the role of Sb. The total group-III flux (Ga plus In) was held constant such that the nitrogen composition remained the same for all samples in this series. The structure for all samples consists of a 7.5 nm GaInNAs(Sb) QW grown on a 300 nm GaAs buffer capped by a 50 nm GaAs layer. All samples were grown at a substrate temperature of 440 °C measured by pyrometry.

A. Varying Sb in the high In regime: The samples contained a single GaInNAs(Sb) QW with nominally 32% In and Sb fluxes which varied between 0 and 1.0×10^{-7} torr BEP. These QWs are typically used for 1.3 μm light emitters and have relatively high amounts of In. The strain in the QWs is large, but usually not large enough to cause the QW to relax. Figure 3(a) shows the HRXRD spectra from these four samples. As will be discussed later, all of the QWs contained 34% indium rather than 32% indium due to flux miscalibration. Curve (i) in Fig. 3(a) represents a GaInNAs QW which is of poor quality. The QW Pendellösung fringes are severely degraded, peak intensity is very low, and strain is much lower than expected. This indicates a loss of structural quality. We believe that the loss of structural quality is associated with phase separation. Such an effect has been observed for this material system by TEM [11, 12]. It has been a challenge to obtain high quality GaInNAs without phase separation at indium compositions greater than 34–35%. Recently, it has been demonstrated that the 3D growth and phase separation can be effectively reduced when GaInNAs is grown at lower temperature (~380 °C) than is typically used during the growth of GaInNAs alloys (460–480 °C). In our case, the 3D growth and phase separation have been reduced by the incorporation of antimony atoms at the growth temperature of 440 °C. Curves (ii), (iii), and (iv) in Fig. 3(a) are from GaInNAsSb QWs which have recovered their structural quality in the presence of an Sb flux. The three spectra, with +2.1% strain, are almost identical except for a very small compressive shift of the QW with increasing Sb flux. For this compositional range of high In and high strain, the addition of Sb greatly improved the structural quality of the GaInNAs. However, from HRXRD, there was no significant difference in the QWs with different Sb fluxes. The compositions were consistent with HRXRD data and simulations. Figure 4(a) shows the In, N, and Sb compositions, which were concluded on the basis of both XRD and SIMS measurements, as a function of the Sb flux. It

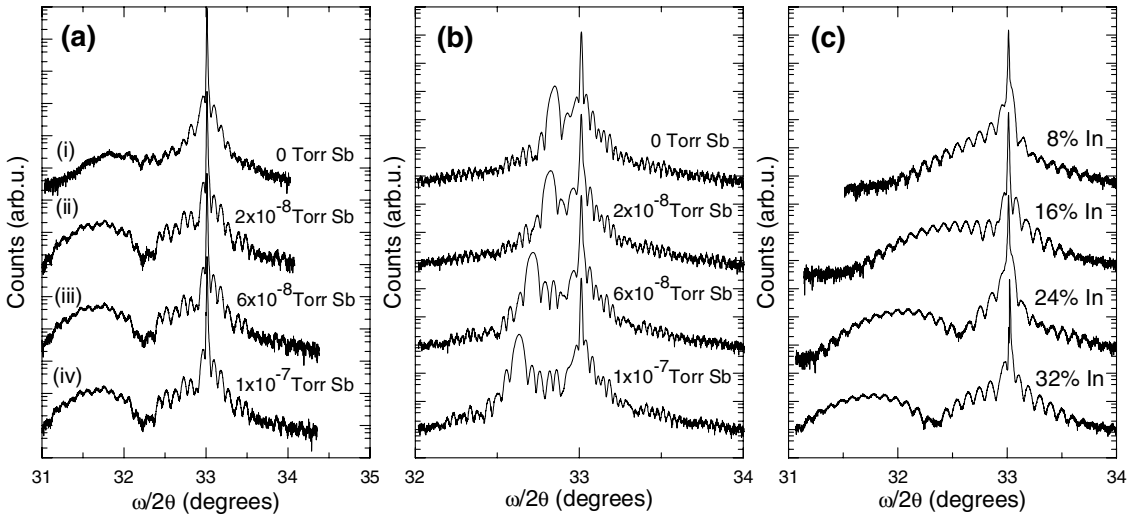

Fig. 3 HRXRD spectra of the (004) GaInNAs(Sb)/GaAs samples with (a) "high" indium composition, (b) "low" indium composition, and (c) varying indium fluxes under a constant antimony flux.

is unclear if the data from the Sb-free GaInNAs sample is believable since the QW itself had phase separated and relaxed, thus changing the bonding structure and possibly the incorporation kinetics of the alloy. The In concentration is much lower than anticipated compared to previous growths which were of good quality. N is also higher than expected compared to past growths and the other three samples which have Sb. Sb enhances N incorporation and has been seen previously in several studies [47, 61–63]. As expected, for increasing Sb fluxes, the Sb concentration in the QW rose from 0.5% to 2.0%. Indium was ~34 % (higher than intended due to flux miscalibration) while nitrogen was 2.3–2.4%. There was not much change in the In or N concentrations with varying Sb flux.

B. Varying Sb in the low In regime: The next series of samples contained relatively low amounts of In (8%) and Sb fluxes which varied between 0 and 1.0×10^{-7} torr BEP. This compositional range is used for

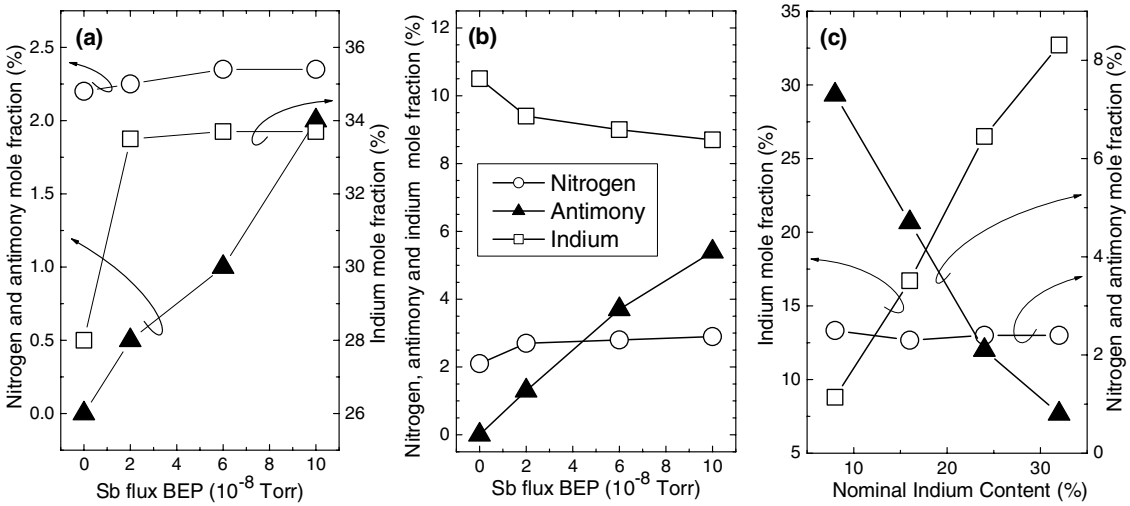

Fig. 4 Indium, nitrogen, and antimony compositions as a function of antimony flux for samples with (a) "high" indium composition and (b) "low" indium composition; (c) nitrogen and antimony compositions as a function of indium concentration with the antimony flux held constant.

solar cell junctions which operate at 1.0 eV. Since thick layers are required for high-efficiency solar cells, the strain must be very small or non-existent and thus contain a much smaller In composition for the same N concentration. For this study both QWs and 1000 Å thick GaInNAs(Sb) layers of identical composition were grown. QW samples were used to study PL whereas the thick layers were used to determine the strain and hence the content of these alloys. The HRXRD spectra of these thicker samples are shown in Fig. 3(b). The HRXRD spectra indicated the samples possessed excellent structural quality. In the Sb-free case, the GaInNAs layer had a strain of +0.24%. The strain increases with larger antimony fluxes, up to +0.54 % with 1.0×10^{-7} torr BEP. Even with the slight increase in strain, these values are significantly lower than highly-strained (2.0–2.6%) QWs which are used for 1.3 μm and 1.55 μm wavelength emission. The compositions of the four samples are shown in Fig. 4(b). As expected, an increase in Sb flux used during the QW growth led to significantly higher Sb incorporation, up to 5.5%. This value is much higher than the high In case, where there was only 2.0% incorporation at the highest Sb flux. N composition was found to be 2.1% in the case without Sb and 2.8% in the presence of Sb. In the Sb-free case, the In composition was found to be 10.5%. However, when 2.0×10^{-8} torr BEP Sb was applied, the composition dropped to 9.4%, even though the In flux was held constant. The In concentration decreased further to 8.7% at the highest Sb flux.

C. Varying In with constant Sb: Finally, in an effort to connect the behaviors observed in the previous two studies, a series of samples was grown with a constant 1.0×10^{-7} torr BEP of Sb while adjusting the In concentration. Figure 3(c) shows the HRXRD spectra taken from the four samples with varying pre-calibrated In concentrations. All the samples have a well defined QW peak and strong Pendellösung fringes, indicating good structural quality. A large change in strain was also observed with the addition of more In, as expected. The strain varied from +0.7% at the low In composition to +2.0% in the high In composition. These values are very similar to those observed in the previous two studies. SIMS and HRXRD were employed to determine the compositions of the samples in this series. A summary of the data is shown in Fig. 4(c). The observed In concentration in the QWs matched well with the intended compositions, determined from previous calibrations. The N composition for all four In compositions remained constant at 2.5%. The total group-III growth rate (In plus Ga) and Sb flux were held constant and thus the relation in Eq. (1) dictates a constant N composition as well. Different In compositions were obtained by changing the ratio of In and Ga fluxes. The Sb concentration decreased with increasing In fluxes down to 0.8% Sb at high In composition. This indicates a very strong interplay of strain, resulting in competition between the In and Sb atoms during growth in decreases Sb incorporation in GaInNAsSb.

In the high In, high strain case, it was unclear whether the presence of Sb leads to a change in In concentration since the Sb-free sample was of poor quality. Ignoring the first sample with poor material quality, there was no observed change in In with increasing Sb flux. It is possible that with such small percentages of Sb incorporation (<2%), any effect on In incorporation would not be detectable. A noticeable change was observed in the low In, low strain case. Increasing Sb flux, the In concentration decreased. The ease of Sb incorporation with low indium concentrations was evident since there was 5.7% Sb compared to 2.0% Sb with high In concentrations for the same maximum flux of Sb. For the samples with constant 1.0×10^{-7} torr BEP of Sb and varying In, the competition between In and Sb was apparent. As the indium increased, the Sb concentration steadily decreased to 0.8%. Additional investigation is required to determine the exact cause of this competition, but it is suspected that the strain associated with large atomic radii of Sb and In in GaAs play a major role. Both atoms induce a large local strain in the GaAs matrix and having both atoms would not be energetically favorable due to the large strain energies they would create. Thus, one species would preferentially incorporate while the other does not. However, the fact that In is a group-III atom and Sb is a group-V atom adds complexity to this argument. At a given N concentration, the increase in strain and decrease in bandgap from Sb and In are comparable for the incorporation of either. Hence, a choice of Sb vs. In will depend on bandgap offsets in device designs.

Since Sb in the GaInNAsSb system also works as a surfactant, it was very important to investigate the profile of Sb concentration in GaInNAsSb/GaAs QWs. Figure 5 shows a SIMS depth profile for an GaInNAsSb/GaAs single QW with high In content, i.e. a highly strained QW where the surfactant effect

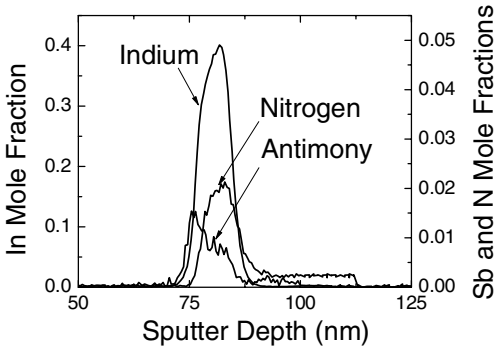

Fig. 5 SIMS profiles of a 1.5 μm GaInNAsSb QW surrounded by GaAs barriers.

should be strongly manifested. Indeed, it is observed that the Sb profile starts later than the nitrogen and indium profiles and that the concentration increases monotonically. Note that the antimony concentration is 1–2%, much higher than a dopant concentration, this demonstrating that antimony is incorporated as a constituent to form a quinary GaInNAsSb alloy.

2.3 Growth and structural characterization of GaInNAsSb/GaNAs/GaAs QWs for long wavelength laser applications

Tensiley-strained GaNAs barriers were adopted relatively early for GaInNAs active regions and were found to substantially increase the number of QWs achievable without relaxation at 1.3 μm [48, 65]. When Sb was added to GaInNAs, the improvement in optical quality was truly amazing. It was thought that adding Sb to the GaNAs barriers should also improve the situation and early 1.5 μm range lasers all employed a GaInNAsSb/GaNAsSb active region [19, 66]. However, it was soon recognized that strain compensation and band offsets were quite unfavorable with GaNAsSb barriers. Finally, successful realization of ~1.5 μm lasers with the lowest threshold current was achieved using GaInNAsSb/GaNAs/GaAs QWs as the active region [22].

In order to achieve the best laser performance, the active part of the laser structure was optimized, i.e. various compositions and thicknesses of GaInNAsSb QW and GaNAs barriers were examined. Because of the complex interaction of bandgap, strain and lattice constant on composition in GaInNAsSb layers, determination of composition is difficult and must be carefully done using several techniques. This issue is discussed in detail elsewhere [4]. Our optimized laser structure, which emits at 1.5 μm, consists of 21 nm thick GaNAs barriers with ~4% N and 7.5 nm thick GaInNAsSb QW with ~38% In, ~3% N and ~2.7% Sb.

In order to investigate possible relaxation and phase separation in GaInNAsSb/GaNAs/GaAs QW structures appropriate XRD and TEM measurements were performed. Figure 6 shows a standard (224) reciprocal space map (RSM) for a representative GaInNAsSb/GaNAs/GaAs QW structure. Any relaxation of the compressively strained QW would result in a diffraction peak located to the lower left of the substrate diffraction peak, while relaxation of the tensile barriers would produce in a peak located to the upper right of the substrate peak. However, no such peaks are present in this figure This demonstrated that there is no relaxation in this QW structure.

Figure 7(a) and (b) show composition sensitive, darkfield 200 TEM images for GaInNAsSb/GaNAs/GaAs QW structures grown at 420 °C and 470 °C, respectively. It is clearly visible that QW interfaces are smooth for the structure grown at the lower temperature. According to the previous discussion, significant deterioration of QW interfaces appear for structures grown at higher temperatures, i.e. at 470 °C in this case. Also for the sample, which was grown at higher temperatures, stronger phase separation was observed in TEM images, see Fig. 7.

The structural quality is strictly correlated with the optical quality of GaInNAsSb QWs. A general trend, which has been observed for GaInNAsSb QW structures, is shown in Fig. 8. The solid

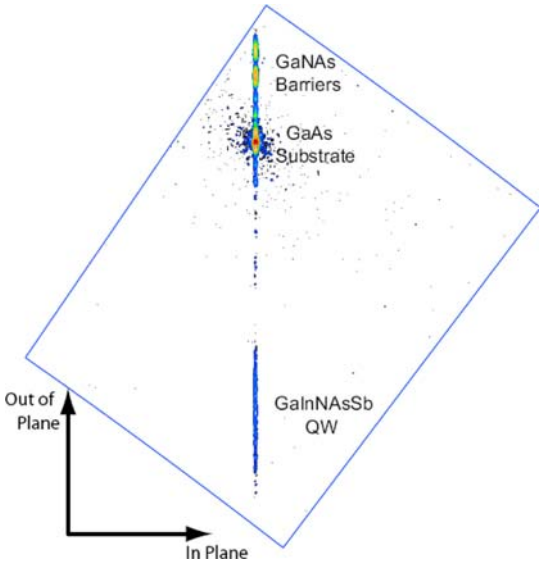

Fig. 6 (online colour at: www.pss-b.com) (224) RSM of the 1.55 μm GaInNAsSb/GaNAs/GaAs QW structure.

squares in this figure show the peak PL intensity as a function of the growth temperature for single $Ga_{0.59}In_{0.41}N_{0.028}$ $As_{0.942}Sb_{0.03}/GaN_{0.03}As_{0.097}$ QWs emitting at 1.55 μm. The arsenic-to-group-III flux ratio was ~10× and the antimony beam-equivalent-pressure was 1.2×10^{-7} torr. The solid dark and grey lines show the observed trends. First, the PL intensity degrades rapidly at low temperatures due to increased point defect formation, most likely arsenic antisites [17], caused by the high arsenic fluxes. Second, the PL intensity also degrades at high temperatures due to phase separation and/or 3D growth. When In or N content is increased the deterioration of PL intensity, which is associated with phase separation/3D growth, appears at lower temperatures as schematically shown in Fig. 8. Adding of antimony allows to avoid the phase separation/3D growth and to increase the growth temperature. Higher growth temperature is recommended for GaInNAsSb due to lower concentration of native point defects and hence higher PL intensity.

3 Band structure

In the case of common III–V semiconductor structures (e.g. InGaAsP/InP, InGaAsP/GaAs or GaInAsSb/GaSb systems), the valence-band offset can be predicted within the so-called "model-solid" theory [67] which yields results for unstrained interfaces. To derive valence-band positions for an alloy, linear interpolation between the binary alloys is appropriate in this case. In order to find the conduction and valence band positions for strained materials, the strain theory for zinc-blende compounds with linear interpolation of strain potentials and stiffness constants for alloys has to be applied. Finally, the bandgap line-up in N-free III–V semiconductor structures can be found with a satisfactory accuracy.

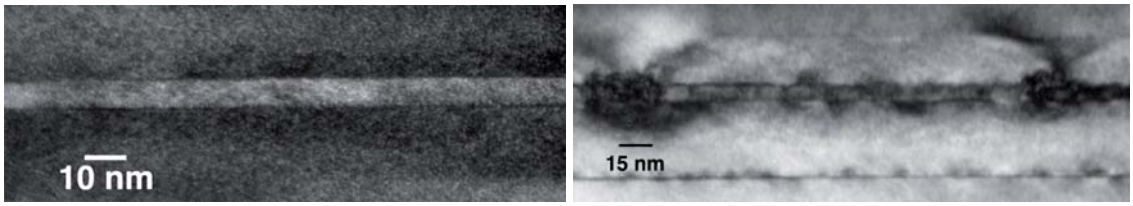

Fig. 7 (online colour at: www.pss-b.com) TEM cross-section image of GaInNAsSb/GaNAs/GaAs QW structure grown at 420 °C (left panel) and 470 °C (right panel).

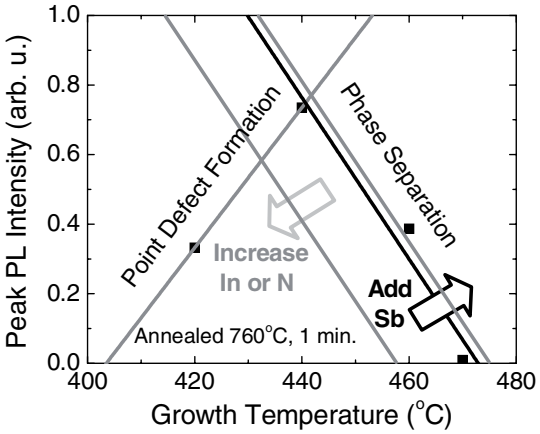

Fig. 8 Room temperature PL intensity of $Ga_{0.59}In_{0.41}N_{0.028}As_{0.942}Sb_{0.03}/GaN_{0.03}As_{0.097}$ QW structures grown at different temperatures, annealed at 760 °C for one minute. The trend is independent of annealing conditions.

In the case of dilute nitrides, this approach does not work correctly. While it is believed that strain theory works satisfactorily for dilute nitrides, it appears difficult to accurately predict the valence band position by model-solid theory. Therefore, the bandgap discontinuity in dilute nitrides was investigated intensively during the last few years. One of the approaches to study this issue in QW structures is electromodulation spectroscopy [68]. This technique, due to its absorption-like character and high sensitivity, probes optical transitions related to the ground and excited states even at room temperature, i.e. the typical operating temperature of electronic devices. The analysis of interband transitions, together with theoretical calculations, makes it possible to determine the energy level structure, including the bandgap discontinuity at QW interfaces. Such an approach has been applied to study the bandgap line-up in our materials, i.e. GaNAsSb/GaAs, GaInNAsSb/GaAs and GaInNAsSb/GaNAs/GaAs step-like QWs [20, 69–72].

The conduction band offset for GaNAsSb/GaAs QWs has been studied in Refs. [69, 70]. It has been found that GaNAsSb/GaAs QWs are Type-I and the conduction band offset (Q_C) for this material system decreases from 80% to 50% when the antimony composition is increased from 0% to 11%. Note that the Q_C is defined before including strain effects using the definition $Q_C = \Delta E_C/(\Delta E_C + \Delta E_V) \times 100\%$ where ΔE_C and ΔE_V are the conduction- and valence-band heterojunction discontinuities for unstrained materials. For QW laser design, the relevant parameters are the bandgap discontinuities in the strained system, namely the values of ΔE_C^*, ΔE_V^{HH} and ΔE_V^{LH} for the conduction, heavy- and light-hole QWs, respectively. A summary of the electron and heavy-hole bandgap discontinuities for GaNAsSb/GaAs QWs, which were studied in Refs. [69, 70], are shown in Fig. 9(a). The ~200 meV deep confinement potential for electrons is attributed to the incorporation of nitrogen atoms into this QW. The incorporation of antimony atoms into GaNAs/GaAs QWs influences mainly the valence band. It shows that GaNAsSb is a very promising compound for bandgap engineering since the bandgap discontinuity can be tuned in a broad range by both nitrogen and antimony compositions. A very similar conclusion has been obtained for GaInNAsSb/GaAs QWs with low indium composition (~10% In, series B in Table 1) [20]. It has been found that the conduction band offset in this system decreases from ~55% to ~45% with the increase in antimony composition from zero to 5.4%. A summary of the band gap discontinuities for this set of GaInNAsSb/GaAs QWs is shown in Fig. 9(b).

For GaInNAsSb/GaAs QWs the concentration of indium atoms can be easily tuned in a broad range (0–40%). It is expected that the indium concentration also influences bandgap discontinuity in this system, an issue studied in Ref. [71]. Obtained results are summarized in Fig. 9(c). It is clearly visible that the change in indium composition influences both the conduction and valence band discontinuities. Unfortunately, for this set of samples the antimony composition is also changing with the indium content increase. However, the antimony-related contribution to the change in Q_C is only a second order effect for these samples since the change in indium composition is much larger than the change in antimony

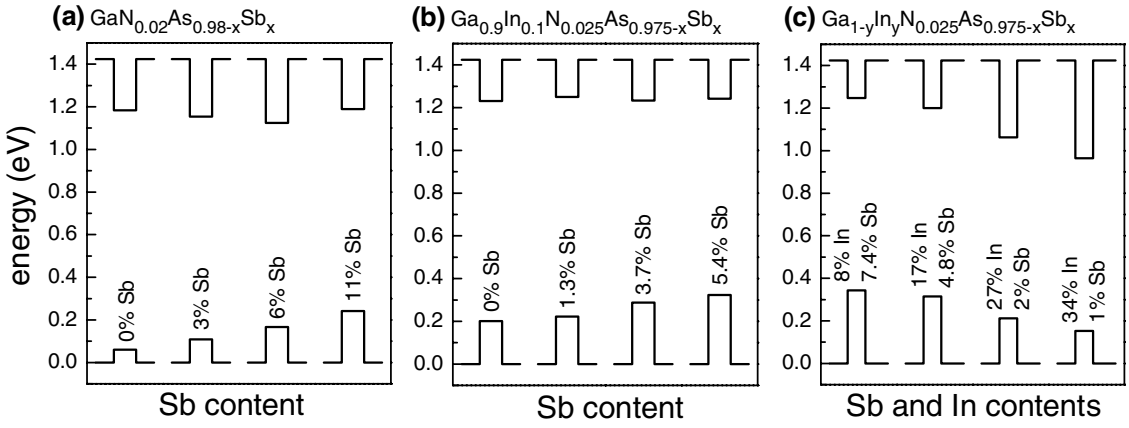

Fig. 9 Bandgap discontinuities for (Ga,In)(N,As,Sb)/GaAs single QWs with various compositions.

composition (8%–34% In vs. 1%–7.4% Sb). Finally, it can be concluded that the incorporation of indium atoms into GaInNAsSb/GaAs QWs influences both the conduction and valence band discontinuities whereas the incorporation of nitrogen atoms influence mainly the conduction band (see band anticrossing model [73]) and the incorporation of antimony atoms influence mainly the valence band [see Fig. 9(b)].

Summarizing, GaInNAsSb/GaAs QWs are a system where the Q_C varies significantly with the alloy composition. This means that GaInNAsSb alloys have significant advantages over ternary and quaternary alloys (InGaAs, GaNAs, or GaInNAs), since the Q_C for the quinary/GaAs system is more tunable than ternary/GaAs or quaternary/GaAs systems. Very often, three parameters in semiconductor structures need to be independently controlled: (i) the bandgap energy, (ii) strain and (iii) bandgap discontinuities. Independent control of the three parameters is impossible for ternary/GaAs and quaternary/GaAs systems, but is possible for quinary/GaAs system if the Q_C is sensitive to the composition of quinary alloys. Our investigations of (Ga,In)(N,As,Sb)/GaAs QWs show that the bandgap discontinuity in this system can be tuned over a broad range. It shows that this material is very promising from the viewpoint of bandgap engineering.

Knowledge of the bandgap discontinuities in (Ga,In)(N,As,Sb)/GaAs system is crucial for optimal design of the active part of a laser structure. A successful realization of ~1.5 μm lasers has been achieved by using a GaInNAsSb/GaNAs QW as the active region. The bandgap line up for this system was investigated by photoreflectance in Ref. [72]. It has been found that this QW has deep enough confinement potential for both electrons and heavy-holes. Currently, there is a pressing need to improve the performance parameters of these lasers, such as the threshold current density and characteristic temperature (T_0), and to push the emission wavelength to 1.6 μm. Therefore, direct investigations of the number of confined states for electrons and holes and the analysis of bandgap line-up in this system are necessary. Recent contactless electroreflectance investigations of the band structure for GaInNAsSb/GaNAs/GaAs QWs with various N content [74, 75] give clear evidence for 11H and 22H transitions in GaInNAsSb/GaNAs QWs (the notation *nm*H denotes the transition between *n*-th heavy-hole valence subband and *m*-th conduction subband). It means that at least two confined state have to exist for both electrons and heavy holes. Figure 10 shows the band structure for GaInNAsSb/GaNAs/GaAs QWs with various nitrogen composition obtained on the basis of matching of experimental data with theoretical calculations. It has been assumed that the best matching for the three samples is when $Q_C \approx 85\%$ and $Q_C \approx 80\%$ for GaInNAsSb/GaAs and GaNAs/GaAs interfaces, respectively. In general, the Q_C for the three samples can vary since the N content for the three samples changes significantly. Finally, it has been concluded that for these samples the variation of Q_C (i.e. (ΔQ_C) is small (probably less than 5%).

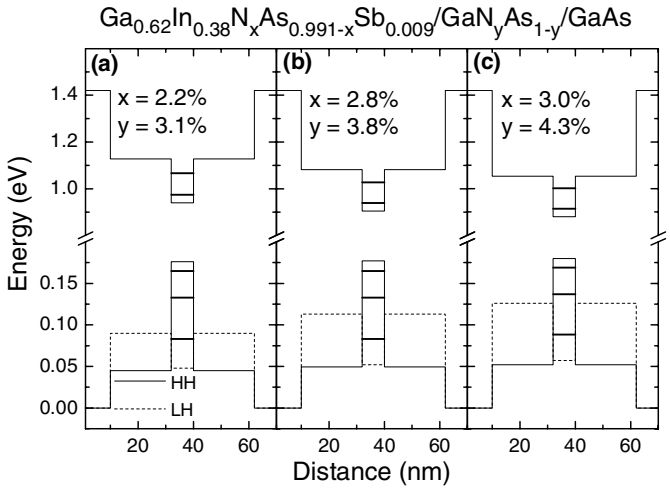

Fig. 10 Energy level structure for $Ga_{0.62}In_{0.38}N_xAs_{0.991-x}Sb_{0.009}/GaN_yAs_{1-y}$/GaAs QW structures with 2.2% and 3.1% of N in GaInNAsSb and GaNAs layers, respectively (a); 2.8% and 3.8% of N in GaInNAsSb and GaNAs layers, respectively (b); 3.0% and 4.3% of N in GaInNAsSb and GaNAs layers, respectively (c). The Q_C for GaInNAsSb/GaAs and GaNAs/GaAs interfaces is assumed as being 85% and 80%, respectively.

Such a small change in the Q_C cannot be determined precisely since the accuracy of the applied method is comparable with this variation.

Figure 10 and our previous investigations let us to formulate following conclusions for GaInNAsSb/GaNAs/GaAs QW system:

(i) increasing N content in the GaInNAsSb layer increases the confinement potential for both electrons and holes, because it reduces the compressive strain in GaInNAsSb layer and it does not change significantly Q_C for GaInNAsSb/GaAs interface in this regime of indium and antimony concentrations;

(ii) increasing N content in GaNAs barriers increases the conduction and valence band discontinuities at GaNAs/GaAs interface and increases the tensile strain in the GaNAs barriers, leading to a decrease of the confinement potential mainly for electrons; in addition it significantly changes the energy difference between the first heavy hole state in GaInNAsSb QW and the light hole subband in GaNAs barriers, see Fig. 10;

(iii) for considered N concentrations, the $Ga_{0.62}In_{0.38}N_xAs_{0.991-x}Sb_{0.009}/GaN_yAs_{1-y}$/GaAs QW structures are Type-I structures with enough deep confinement potentials for both electrons and heavy holes, i.e. these potentials confine at least two states.

The two first conclusions, (i) and (ii), give some directions in the optimization of T_0 in GaInNAsSb/GaNAs/GaAs based lasers while the last conclusion confirms that there is a window for N content where GaInNAsSb/GaNAs QWs have enough deep confinement potential for both electrons and holes.

4 Optical properties

Investigations of the optical quality for GaInNAsSb-based QWs are focused on PL measurements, since this technique is very sensitive to defect states. This is in contrast to electromodulation spectroscopy, which is sensitive mostly to the band structure, i.e. the density of states. PL measurements are usually performed at room temperature, since it is the operating temperature for optoelectronic devices, and at this temperature, the non-radiative processes are strongly manifested. Post growth *ex situ* annealing typically improves the optical properties of dilute nitrides and is a standard step in the fabrication of GaInNAsSb-based lasers. The changes that occur during annealing are complex and not fully under-

stood. It is generally accepted that low luminescence efficiency in as-grown material is the result of non-radiative recombination centers or traps inside the bandgap of dilute nitrides. Many different traps likely exist inside the bandgap of dilute nitrides, depending upon the growth method, growth conditions, and alloy composition. The exact nature of these centers is still unknown. Annealing increases the luminescence efficiency by decreasing the concentration of these centers. Thus the optimization of annealing process in dilute nitrides is a very important issue in the fabrication of high quality materials for laser applications. Unfortunately, the PL undergoes a blue shift during the thermal treatment, increasing the difficulty of reaching longer wavelengths. This phenomenon is associated with (i) changes in the nitrogen nearest neighbour environments [76–80] (ii) a reduction of tails of the density of state [81] as well as (iii) some atom interdiffusion across QW interfaces for samples annealed at higher temperatures [78]. Recent systematic investigations [82] evidently demonstrate that the blue shift observed after low temperature annealing (<750 °C) is clearly identified to originate mainly from atomic reorganization while the interdiffusion process occurs after high temparature annealing (>750 °C). For reasonable annealing conditions the blueshift saturates and is usually less than 80 nm. Therefore, this effect is not a huge obstacle for reaching longer wavelengths. In order to improve performances of 1.5 μm lasers, a systematic investigation of optimum growth and annealing conditions was performed.

4.1 Photoluminescence of GaInNAsSb quantum wells of widely varying compositions

When antimony was first added to GaInNAs to improve the material quality, little attention was given to the amount used, in which situations it would be beneficial, or how it worked. In order to understand the surfactant role of antimony, PL measurements were performed for the series of GaInNAsSb QWs of widely varying composition [27]. It has been observed that for samples with high indium, and thus high strain, adding antimony improved the structural and optical quality of GaInNAs. However, the addition of any antimony to the low indium, low strain GaInNAs degraded the optical quality. This means that for the thick lattice matched layers used in GaInNAs solar cells, the strain is minimal or zero and a surfactant is undesirable. In addition, it has been observed that the optimal annealing temperature is strongly correlated with strain due to compositional differences for each of series of GaInNAs(Sb) samples [83]. When antimony content is increased in GaInNAsSb QWs with low indium content, the lattice strain increased and the optimal annealing temperature correspondingly decreased. The same effect was observed for GaInNAsSb QWs with increasing indium content (samples C in Table 1). This leads to a conclusion that a different optimum annealing cycle is expected for different compositions of GaInNAsSb alloys.

4.2 Growth optimization of long wavelength GaInNAsSb/GaNAs quantum well structures

In order to improve laser performance, room temperature PL measurements were performed for GaInNAsSb/GaNAs/GaAs QW structures grown at different temperatures [84], under different arsenic and antimony fluxes [85], and annealed under different conditions [86].

Growth temperature: As was mentioned (see Fig. 8), the temperature is one of the most critical growth parameters for producing high quality dilute-nitrides. PL intensity degraded rapidly at low temperatures due to increased point defect formation, most likely arsenic antisites, caused by the high arsenic fluxes (the arsenic-to-group-III flux ratio was ~10× and the antimony beam-equivalent-pressure was 1.2×10^{-7} torr). Phase separation and/or three-dimensional growth limit the maximum growth temperature. Strong evidence of phase separation at high growth temperature has been found in TEM studies for GaInNAs [89]. Also for GaInNAsSb/GaNAs/GaAs QW structures, the phase separation and/or three-dimensional growth appear for samples grown at higher temperatures, see right panel in Fig. 7. Phase separation manifests itself as nano-scale lateral compositional fluctuations of alternating indium-rich (nitrogen-poor) and nitrogen-rich (indium-poor) regions. The resulting growth temperature window is quite narrow, ~20 °C for 1.55 μm range GaInNAs [17]. In the case of the GaInNAsSb system, the growth window is also narrow, but is observed at higher temperatures ~440 °C. Therefore, it is easier to

grow GaInNAsSb material in the 1.55 μm range with good optical quality, i.e. QWs with relatively low number of point defects, which are the source of non-radiative recombination. Sufficient control of the growth temperature, ±3 °C, is easily achieved in MBE growth with careful pyrometry or band-edge thermometry measurements.

Arsenic flux: High quality dilute nitrides for $\lambda \leq 1.3$ μm are typically grown under relatively high arsenic fluxes, As/group-III flux of ~10× [5]. However, in order to extend the wavelength beyond 1.3 μm, very low temperature (320~350 °C) and lower, very precisely controlled As fluxes had to be used for 1.55 μm GaInNAs active regions [17]. This growth regime is at/near the stoichiometric limit, and is quite difficult to control and reproducibility is a significant challenge. By contrast, GaInNAsSb can be grown at significantly higher temperatures and with a much broader range of arsenic fluxes. We have observed that a wide range of arsenic fluxes produced both stable optical intensity and emission wavelength. Therefore, high quality GaInNAsSb active layers can be grow repeatably and reliably with very little concern for the accuracy of the arsenic flux [85].

Antimony flux: The antimony flux is a moderately important consideration. The surfactant effect of antimony is to limit the surface diffusion length (SDL) of the incident adatoms, particularly indium, thereby inhibiting phase separation and roughening. On the other hand, if the antimony flux is too high, the SDL becomes too short, and adatoms will not be able to find optimal lattice sites, resulting in degraded crystal quality. Therefore, an optimal antimony flux is observed when all other growth parameters are held constant [89]. The optimal antimony flux likely depends on the substrate temperature, nitrogen content, indium content, and the growth rate [27, 85, 90]. However, only moderate (±10%) control of the antimony flux is required to achieve optimal quality.

Nitrogen flux: Reactive nitrogen is supplied by a nitrogen plasma source. Careful control of the nitrogen plasma is critical in producing high quality dilute nitrides. We have found that material quality depends very strongly on both the level of residual contaminants and ion bombardment from the plasma [7]. The nitrogen plasma has many adjustable parameters, such as crucible design, operating pressure and rf power. Each of these parameters can affect the source operation and the quality and composition of the material in very subtle and interrelated ways. We found a very stable and reproducible saddle point for operation of our nitrogen source and when operated there, the nitrogen composition was inversely proportional to the group-III growth rate, when other nitrogen plasma parameters were held constant. As a result, we control the nitrogen content of all epitaxial films by directly controlling group-III growth rate and not by varying the plasma conditions.

Despite the anticipated complexity from the many variables involved in the growth of quinary alloys, 1.5–1.6 μm lasers with high performances, which contain GaInNAsSb/GaNAs/GaAs QW in the active part, can be grown with excellent repeatability in wavelength and optical quality with only adjustment of the Ga and In fluxes [91]. Our optimum growth conditions include keeping the nitrogen plasma parameters and Sb flux constant, adjusting the group-III fluxes for the desired ratio and N composition, and

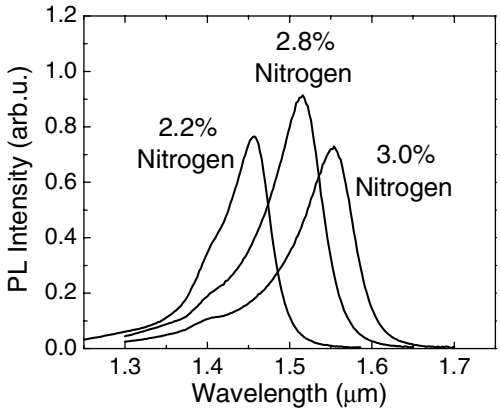

Fig. 11 PL intensity as a function of the nitrogen content, under (identical) optimal annealing conditions [85]. No trend in the optical quality is observed.

carefully controlling the growth temperature. All these requirements can be easily met with the current state of MBE technology. Most importantly, the emission wavelength can be easily increased without any quality degradation, by simply reducing the growth rate to add more nitrogen [89]. Figure 11 shows annealed PL spectra of samples with increasing nitrogen content [85]. The emission wavelength is increased without degradation in PL intensity. This powerful result shows that emission wavelength can be tuned across the entire 1.55 μm band changing only SINGLE variable – the total growth rate – and does not require complicated reoptimization of any other growth parameters. This result is very striking, in that it runs contrary to all earlier reports of rapid degradation with increasing nitrogen content. We have found that adding more nitrogen is a better way of extending laser wavelength than adding indium [86], resulting in the lowest threshold 1.55 μm dilute nitride lasers to date.

5 Applications

The main driving force for the exploration of quinary GaInNAsSb alloys was the application of this material to long-wavelength lasers. However, there are still a number of challenges that must be over come to realize the full potential of this new materials system. The large parameter space with quaternary and quinary materials, which allows both bandgap and strain engineering of devices, creates large area for exploration. Currently, this material has a real application in long-wavelength lasers [6, 7, 21–25, 89]. In addition, GaInNAs(Sb) is promising in solar cell applications and mid-infrared applications. Some examples are given in this section.

5.1 GaInNAsSb long-wavelength VCSELs

GaAs-based VCSELs are the dominant technology in transmitters for high performance, short-range datalinks and optical network switches due to their low cost, ease of fibre coupling, and straightforward fabrication of large multi-element 2D arrays. At Stanford [92–94], we chose a design much like that used in the 850 nm VCSELs, where the mirrors are doped, one n-type and the other p-type, with the current driven through the mirrors. The VCSEL structure consist of three 7 nm thick $Ga_{0.62}In_{0.38}N_{0.016}As_{0.958}Sb_{0.026}$ QWs with 20 nm thick GaNAs barriers. Other relevant details are given in Ref. [95]. Figure 12 shows the fiber-coupled spectrum at 500 and 800 mA of peak current, showing the onset of stimulated emission. The VCSELs were pulsed at 0.1% duty cycle, with 2 μs pulses at a 500 Hz repetition rate. Multiple transverse modes are visible above threshold, due to the large 66 μm diameter current aperture of the VCSELs. The threshold current, I_{th}, was 543 mA (pulsed), corresponding to current density, J_{th} of 16 or 5.3 kA/cm^2 per QW. The VCSEL QWs were identical to the single QW from our earlier CW 1.49 μm edge emitting lasers. Due to lower operating temperature (–10 °C) and short cavity, the

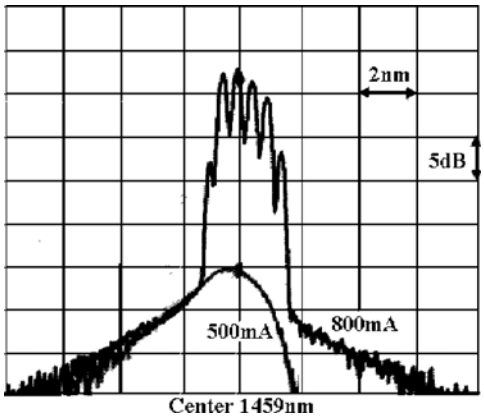

Fig. 12 Spectra of the first monolithic $\lambda > 1.45$ μm VCSEL on GaAs operating just below and about 1.6× threshold.

VCSELs lased at 1.46 μm, a significantly shorter wavelength. It is expected that even a simple improvement in mounting technique would reduce the need for cooling the devices. This is the first reported monolithic VCSEL grown on GaAs to lase at wavelengths greater than 1.45 μm [22, 95, 96].

5.2 GaInNAsSb high power edge-emitting lasers

High-power (>500 mW) single-mode lasers are highly desirable as pumps for Raman fibre amplifiers and many nonlinear channel switching applications in optical networks. While VCSELs at 1.3 μm are extremely useful for metro area networks and local area networks, Raman pump lasers must work at 1.45 μm to be useful in combination with Er-doped fibre amplifiers at 1.55 μm and over 1.2–1.5 μm range to provide amplifiers over the entire low-loss fibre region. In our case the lasing wavelength was successfully extended to 1.55 μm by increasing the nitrogen content [89]. It is worth noting that our initial attempts to extend the wavelength by increasing indium content were less successful, resulting in higher threshold current density, even though the optical quality of the PL sample was equivalent [86]. We suggest that the higher-indium GaInNAsSb active regions are damaged by the in-situ anneal during laser growth, and their weak thermal robustness is evidenced by the lower optimal anneal temperature of the PL samples. Adding more nitrogen enabled us to increase the laser wavelength without compromising thermal robustness of the QW [89].

Utilizing our improved growth conditions and deflection plates on the nitrogen plasma cell, we reported the lowest threshold, long-wavelength lasers on GaAs with a threshold current density (J_{th}) of 579 A/cm^2 and an external efficiency (η_e) was 40% [96]. The characteristic temperatures for the threshold current density (T_0) and external efficiency (T_1) were 71 and 171 K, respectively, near room temperature. The threshold current density of 1.55 μm lasers was further reduced by deeper ridge etching through the GaAs waveguide layer [80, 97]. All previous lasers from our group were etched to near the interface between the upper AlGaAs cladding and the GaAs waveguide. Deeper etching enabled the lasers to exhibit substantially lower threshold current of 318 A/cm^2 under pulsed operation. The CW J_{th} was only 373 A/cm^2 and η_e and was 41%, as seen in Fig. 13. An optical spectrum taken at 1.3x threshold is shown in the inset, showing lasing at 1.54 μm. Peak output powers were 650 mW (current driver-limited) and 250 mW under pulsed and CW operation, respectively. These laser thresholds are only ~50% higher than the best devices reported for dilute-nitride lasers at 1.3 μm [98] and comparable to the best reports beyond 1.3 μm [99], despite the increased Auger recombination and inter-valence band absorption caused by the longer emission wavelength, as well as the substantially greater nitrogen content (~6× increase). We suppose that the small energy difference between light-holes in GaNAs barriers and the ground heavy-hole state in GaInNAsSb QW (see Fig. 10) could be one of the reasons for the observed low characteristic temperature T_0 in these lasers.

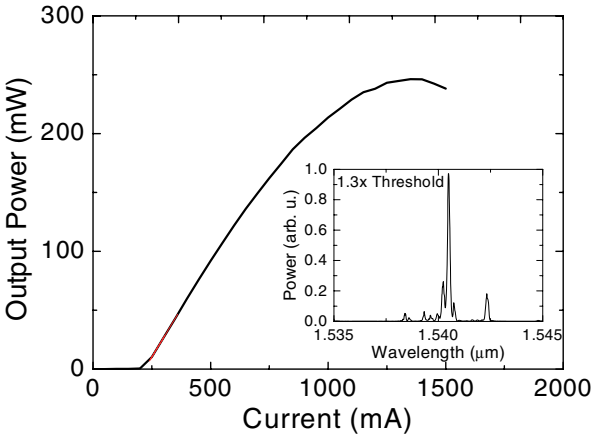

Fig. 13 (online colour at: www.pss-b.com) CW L–I and optical spectrum (inset) of a 1.55 μm active region laser with ridge etching through the QW.

5.3 GaInNAsSb electroabsorption modulators and saturable absorbers

For very high speed optical communication systems, direct modulation of the laser source is often infeasible or impractical and external modulators are required. Also, saturable absorbers are important elements in high-speed systems, providing a gain modulating medium for mode locking lasers. Thus both modulators and saturable absorbers may become important components of future high-speed optical interconnects used to overcome the limiting RC delays in microprocessor back-ends. Recent work in our group [100] has shown that GaInNAsSb QWs show very large absorption swings due to the quantum confinement Stark effect; hence, they have much potential for use in optical modulators in the 1.3–1.6 μm wavelength range. Recently, Du et al. [101] have demonstrated a saturable absorber at 1.5 μm utilizing GaInNAsSb-GaNAs system. Thus, we believe that quinary GaInNAsSb alloys have potential in this field.

5.4 GaInNAs(Sb) solar cells

GaInNAs has garnered great interest as material for use in multijunction solar cells [10]. Before GaInNAs, GaAs-based devices requiring thick layers of 1 eV bandgap material necessitated techniques such as graded strain relaxation layers or wafer bonding that introduced performance degrading defects. The ability to grow thick coherent layers (~1 μm) is extremely important for high-quality absorption-based devices, such as solar cells and detectors. With concentrations of 6–8% indium and 2–3% nitrogen, GaInNAs has a bandgap of 1.0 eV with little or no strain when grown on GaAs. Analyzing PL intensity, antimony has been found detrimental to GaInNAs material with low concentrations of indium and low lattice strain contrary to the behavior of alloys with high indium and high strain [27]. However, the intensity decreases only three times [27] and it is well known that PL intensity is not a good metric of potential device performance for solar cells. Moreover, the quality of this material can be improved by better optimization of the growth conditions, such as was done for 1.5 μm lasers. Thus GaInNAsSb alloys are a viable option for the 1.0 eV junction in a four junction solar cell. In addition, the further reduction of the bandgap with the incorporation of antimony permits the creation of three junction solar cells with a 0.9 eV GaInNAsSb subcell replacing the germanium subcell. Such a triple junction device could permit the creation of a solar cell with greater than 40% efficiency [102].

Recently, the first GaInNAsSb solar cells were produced, which had narrow 0.92 eV bandgaps and maintained high internal quantum efficiency [103]. Table 2 summarizes dilute nitride solar cells from the literature, including the short-circuit current that would be obtained beneath a GaAs sub-cell in a monolithic multijunction stack. The GaInNAsSb device represents one of the smallest bandgaps achieved in a dilute nitride solar cell with high quantum efficiency, and as a result displays a substantially higher short-circuit current density than could be achieved previously. Inadequate short-circuit current in dilute nitride subcells has been the largest barrier to their success in multijunction devices.

Table 2 Bandgap, internal quantum efficiency (at 0.2 eV above the bandgap), and short-circuit current underneath a GaAs subcell in a monolithic multijunction device [104].

sample	reference	bandgap (eV)	IQE (E_g + 0.2 eV)	J_{sc} (mA/cm^2)
GaInNAsSb	[103]	0.92	0.72	14.8
GaInNAs	[103]	1.03	0.64	9.03
GaInNAs	[105]	1.04	0.74	9.64
GaInNAs	[106]	1.15	0.96	9.38
GaInNAs	[107]	1.07	0.78	9.26
GaInNAs	[108]	1.0	0.55	8.95
GaInNAs	[108]	1.1	0.67	7.79

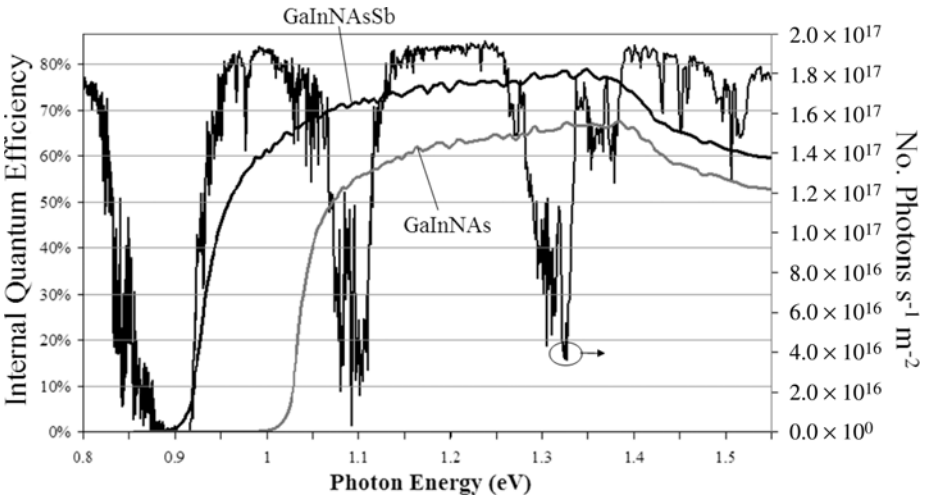

Fig. 14 Internal quantum efficiency spectra of GaInNAs and GaInNAsSb solar cells, overlaid on the AM1.5 low-AOD solar spectrum.

Figure 14 plots the internal quantum efficiency of a GaInNAs and GaInNAsSb solar cell, overlaid on top of the AM1.5 low-AOD solar spectrum. The internal quantum efficiency of the dilute nitride antimonide device, 79% at maximum, is higher than that of the GaInNAs cell mainly due to wider depletion widths caused by lower background carrier concentrations in the unintentionally doped regions of the device [103]. The narrow bandgap allows this subcell to absorb more of the solar spectrum, which, coupled with the high quantum efficiency provides this device with a large short-circuit current. It is interesting to note that subcells with bandgaps slightly lower than 0.92 eV would not produce much additional photocurrent since there is an atmospheric absorption band between 0.85 and 0.92 eV in the AM1.5 solar spectrum.

The GaInNAsSb device in Fig. 14, if underneath a GaAs sub-cell in a multijunction structure, would produce a short-circuit current density of 14.8 mA/cm^2 [103], determined using the quantum efficiency and the low-AOD spectrum truncated at 880 nm. The GaInNAs device in Fig. 14 would have a short-circuit current density of 9.0 mA/cm^2 under the same conditions, which is typical of dilute nitride devices in the literature (Table 2). The current world record lattice-matched triple-junction device composed of GaInP/InGaAs/Ge (39% efficiency), has a short-circuit current density of 3.377 A/cm^2 at 236-suns concentration, which corresponds to 14.3 mA/cm^2 at 1-sun [109]. This indicates that the narrow bandgap GaInNAsSb cell has large enough photoresponse to current match the upper subcells in a state of the art multijunction device. The fill-factor and open-circuit voltage of these un-optimized GaInNAsSb devices were roughly 0.6 and 280 mV (at 1-sun) [103], which is equal to or better than those values in high-quality Ge solar cells [110]. It is expected that the fill-factor and open-circuit voltage can be improved with further optimization of materials quality and device structure.

5.5 Mid infrared applications

Incorporating nitrogen into narrow gap materials (InAs or InAsSb) is very attractive because it can reduce the energy gap and enable emission beyond the far-infrared, a feat not possible with conventional III–V semiconductors, see Fig. 1. In addition, nitrogen in these materials will increase the electron effective mass, suppressing Auger recombination. To date there are very few reports of dilute nitrides development in narrow gap materials [111–113]. Our recent investigations in this field show that it was much easier to grow good quality quaternary alloys (InNAsSb) than ternary alloys (GaNSb or InNSb) [114]. Thus we believe that quaternary and quinary alloys containing nitrogen have some potential in this field.

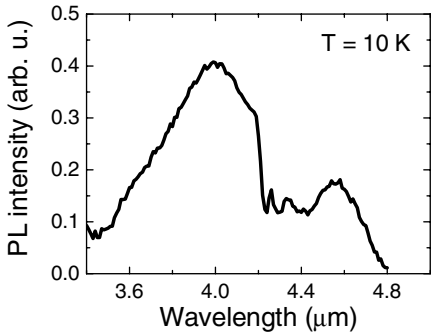

Fig. 15 10 K PL spectrum of an InNAsSb/InAs SQW.

Recently, we successfully grew InNAsSb layers and QWs [114, 115]. These samples were investigated by HRXRD, SIMS and PL. Distinct Pendellösung fringes and well defined peaks were observed for these samples that indicate good structural quality, i.e. no severe structural defects caused by relaxation or phase separation. The nitrogen and antimony concentrations have been found to be 1% and 13%, respectively. Figure 15 shows PL spectrum from 9 nm thick InNAsSb/InAs single QW. The peak intensity is located at a wavelength of ~4 μm. There is a strong atmospheric absorption at 4.2–4.5 μm attributed to the presence of CO_2 in the environment during the measurements. These results illustrate the potential of III–V compounds (dilute nitride narrow bandgap materials) for mid infra-red and far infra-red biosensing devices.

6 Conclusion and outlook

It is clear that the quinary alloy, GaInNAsSb is a complex materials system. Many different growth parameters can affect one another, but our systematic study has provided insights that demonstrate that growth in a broad, relatively easily controlled growth regime is possible. Thus the answer for our old question: "*is this quinary alloy a prototype system that provides the ultimate opportunity for bandgap engineering and novel devices, or is a recipe for a disaster of poorly controlled and non-reproducible epitaxial growth?*" is that this material is complex, but can be reproducibly controlled by present MBE technology.

The major challenge of this materials system has been to understand the differences of dilute nitrides compared to other III–V alloys and to produce low threshold lasers at any desired wavelength between 1.3 and 1.6 μm. We believe that GaInNAsSb on GaAs will be the foundation technology that will enable low cost, wide bandwidth MAN/LAN/SAN networks, optical switching and routers. The newest versions of production MBE systems, with their greater versatility in number of liquid metal sources, could easily change the production role of MBE. The advances in equipment, combined with the significantly easier growth of GaInNAsSb by MBE, will likely make MBE the choice for production of VCSELs, high power edge emitting lasers and photonic integrated circuits. Progress has been rapid for such a complex materials system and the potential for use in high-speed networks is indeed bright.

The discovery that antimony is incorporated as a constituent, which mainly modifies the valence band, opens an additional means to optimize optoelectronic devices and provide opportunities for bandgap engineering and novel devices. We believe that this feature of GaInNAsSb alloys can be a driving force to explore new material compositions and new device concepts. The growth of new dilute nitrides (InNAs, GaNSb, InNSb, InNAsSb) and GaInNAsSb alloys with different substrates and available bandgaps represents new opportunities and challenges for MBE technology.

Acknowledgements The authors acknowledge the support under DARPA and ARO contracts MDA972-00-1-024, DAAD17-02-C-0101 and DAAD199-02-1-0184, ONR contract N00014-01-1-00100, as well as the Stanford Network Research Center (SNRC). In addition, R.K. acknowledges the support from Foundation for Polish Science.

References

[1] I. A. Buyanova and W. M. Chen, Physics and applications of dilute nitrides (Taylor & Francis Books, Inc., New York, 2004).
[2] M. Henini, Dilute nitride semiconductors (Elsevier Ltd, Oxford, 2005).
[3] M. Kondow, K. Uomi, A. Niwa, T. Kitatani, S. Watahiki, and Y. Yazawa, Jpn. J. Appl. Phys., Part 1 **35**, 1273 (1996).
[4] J. S. Harris Jr., IEEE J. Sel. Top. Quantum Electron. **6**, 1145 (2000).
[5] J. S. Harris Jr., Semicond. Sci. Technol. **17**, 880 (2002).
[6] J. S. Harris Jr., J. Cryst. Growth **278**, 3 (2005).
[7] M. A. Wistey, S. R. Bank, H. B. Yuen, H. P. Bae, and J. S. Harris Jr., J. Cryst. Growth **278**, 229 (2005).
[8] H. B. Yuen, M. A. Wistey, S. R. Bank, H. P. Bae, and J. S. Harris Jr., J. Vac. Sci. Technol. B **23**, 1328 (2005).
[9] A. J. Ptak, S. W. Johnston, S. Kurtz, D. J. Friedman, and W. K. Metzger, J. Cryst. Growth **251**, 392 (2003).
[10] S. R. Kurtz, A. A. Allerman, E. D. Jones, J. Gee, J. J. Banas, and B. E. Hammons, Appl. Phys. Lett. **74**, 729 (1999).
[11] K. Volz, T. Torunski, and W. Stolz, J. Appl. Phys. **97**, 014306 (2005).
[12] X. Kong, A. Trampert, E. Tournie, and K. H. Ploog, Appl. Phys. Lett. **87**, 171901 (2005).
[13] M. Fisher, M. Reinhardt, and A. Forchel, Electron. Lett. **36**, 1208 (2000).
[14] M. Fisher, M. Reinhardt, and A. Forchel, IEEE J. Sel. Top. Quantum Electron. **7**, 149 (2001).
[15] D. Gollub, S. Moses, M. Fisher, M. Kamp, and A. Forchel, Electron. Lett. **40**, 427 (2004).
[16] M. Hugues, B. Damilano, J. Barjon, J.-Y. Duboz, J. Massies, J.-M. Ulloa, M. Montes, and A. Hierro, Electron. Lett. **41**, 595 (2005).
[17] G. Jaschke, R. Averbeck, L. Geelhaar, and H. Riechert, J. Cryst. Growth **278**, 224 (2005).
[18] X. Yang, M. J. Jurkovic, J. B. Heroux, and W. I. Wang, Appl. Phys. Lett. **75**, 178 (1999).
[19] W. Ha, V. Gambin, S. Bank, M. Wistey, H. Yuen, S. Kim, and J. S. Harris Jr., IEEE J. Quantum Electron. **38**, 1260 (2002).
[20] R. Kudrawiec, M. Motyka, M. Gladysiewicz, J. Misiewicz, H. B. Yuen, S. R. Bank, H. Bae, M. A. Wistey, and J. S. Harris, Appl. Phys. Lett. **88**, 221113 (2006).
[21] S. R. Bank, M. A. Wistey, L. L. Goddard, H. B. Yuen, V. Lordi, and J. S. Harris Jr., IEEE J. Quantum Electron. **40**, 656 (2004).
[22] M. A. Wistey, S. R. Bank, H. B. Yuen, L. L. Goddard, and J. S. Harris Jr., Electron. Lett. **39**, 1822 (2003).
[23] S. R. Bank, L. L. Goddard, M. A. Wistey, H. B. Yuen, and J. S. Harris Jr., IEEE J. Sel. Top. Quantum Electron. **11**, 1089 (2005).
[24] J. A. Gupta, P. J. Barrios, X. Zhang, J. Lapointe, D. Poitras, G. Pakulski, X. Wu, and A. Delâge, Electron. Lett. **41**, 1060 (2005).
[25] S. R. Bank, H. P. Bae, H. B. Yuen, M. A. Wistey, L. L. Goddard, and J. S. Harris, Electron. Lett. **42**, 156 (2006).
[26] Z. C. Niu, S. Y. Zhang, H. Q. Ni, D. H. Wu, H. Zhao, H. L. Peng, Y. Q. Xu, S. Y. Li, Z. H. He, Z. W. Ren, Q. Han, X. H. Yang, Y. Du, and R. H. Wu, Appl. Phys. Lett. **87**, 231121 (2005).
[27] H. B. Yuen, S. R. Bank, H. Bae, M. A. Wistey, and J. S. Harris Jr., J. Appl. Phys. **99**, 093504 (2006).
[28] E. Tournie, M. A. Pinault, S. Vezian, J. Massies, and O. Tottereau, Appl. Phys. Lett. **77**, 2189 (2000).
[29] C. W. Tu, J. Phys.: Condens. Matter **13**, 7169 (2001).
[30] M. Kondow and T. Kitatani, Semicond. Sci. Technol. **17**, 746 (2002).
[31] J.-C. Harmand, A. Caliman, E. V. K. Rao, L. Largeau, J. Ramos, R. Teissier, L. Travers, G. Ungaro, B. Theys, and I. F. L. Dias, Semicond. Sci. Technol. **17**, 778 (2002).
[32] E.-M. Pavelescu, T. Jouhti, C. S. Peng, W. Li, J. Konttinen, M. Dumitrescu, P. Laukkanen, and M. Pessa, J. Cryst. Growth **241**, 31 (2002).
[33] M. Fisher, D. Gollub, M. Reinhardt, M. Kamp, and A. Forchel, J. Cryst. Growth **251**, 353 (2003).
[34] J.-M. Chauveau, A. Trampert, M.-A. Pinault, E. Tournie, K. Du, and K. H. Ploog, J. Cryst. Growth **251**, 383 (2003).
[35] H. L. Liu, M. Hopkinson, P. Navaretti, M. Gutierrez, J. S. Ng, and J. P. R. David, Appl. Phys. Lett. **83**, 4951 (2003).
[36] J. A. Gupta, G. I. Sproule, X. Wu, and Z. R. Wasilewski, J. Cryst. Growth **291**, 86 (2006).
[37] F. Ishikawa, M. Horicke, U. Jahn, A. Trampert, and K. H. Ploog, Appl. Phys. Lett. **88**, 191115 (2006).

[38] J. F. Geisz, D. J. Friedman, J. M. Olson, S. R. Kurtz, and B. M. Keyes, J. Cryst. Growth **195**, 401 (1998).
[39] Z. Pan, T. Miyamoto, D. Schlenker, S. Sato, F. Koyama, and K. Iga, J. Appl. Phys. **84**, 6409 (1998).
[40] J. Derluyn, I. Moerman, M. R. Leys, G. Patriarche, G. Sek, R. Kudrawiec, W. Rudno-Rudzinski, K. Ryczko, and J. Misiewicz, J. Appl. Phys. **94**, 2752 (2003).
[41] J.-Y. Yeh, N. Tansu, and L. J. Mawst, Electron. Lett. **40**, 739 (2004).
[42] W. C. Chen, Y. K. Su, R.W. Chuang, and S. H. Hsu, J. Vac. Sci. Technol. A **24**, 591 (2006).
[43] J. Neugebauer and C. G. Van de Walle, Phys. Rev. B **51**, 10568 (1995).
[44] S.-H. Wie and A. Zunger, Phys. Rev. Lett. **76**, 667 (1996).
[45] Y. Qiu, S. A. Nikishin, H. Temkin, V. A. Elyukhin and Yu. A. Kudriavtsev, Appl. Phys. Lett. **70**, 2831 (1997).
[46] E. Tournie, N. Grandjean, A. Trampert, J. Massies, and K. H. Ploog, J. Cryst. Growth **150**, 460 (1995).
[47] J. C. Harmand, G. Ungaro, L. Largeau, and G. LeRoux, Appl. Phys. Lett. **77**, 2482 (2000).
[48] S. G. Spruytte, M. C. Larson, W. Wampler, C. W. Coldren, H. E. Petersen, and J. S. Harris Jr., J. Cryst. Growth **227/228**, 506 (2001).
[49] S. G. Spruytte, MBE growth of Nitride-Arsenides for Long-wavelength Opto-electronics, PhD Thesis, Stanford University (2001).
[50] G. B. Stringfellow, Organometallic Vapour-Phase Epitaxy: Theory and Practice (Academic, Boston, 1989), p. 123.
[51] R. R. LaPierre, B. J. Robinson, and D. A. Thompson, J. Appl. Phys. **79**, 4068 (1996).
[52] A. Mereuta, G. Saint-Girons, S. Bouchoule, I. Sagnes, F. Alexandre, G. Le Roux, J. Decobert, and A. Qugazzaden, Opt. Mater. **17**, 3516 (2001).
[53] S. Spruytte, W. Wampler, P. Krisprin, C. Coldren, M. Larson, K. Ploog, and J. S. Harris, J. Appl. Phys. **89**, 6294 (2001).
[54] H. P. Xin and C. W. Tu, Appl. Phys. Lett. **72**, 2442 (1998).
[55] Z. Sun, S. F. Yoon, K. C. Yew, W. K. Loke, W. Fan, S. Wang, and T. K. Ng, J. Appl. Phys. **94**, 1069 (2003).
[56] F. Ishikawa, E. Luna, A. Trampert, and K. H. Ploog, Appl. Phys. Lett. **89**, 181910 (2006).
[57] A. Hasse, K. Volz, A. K. Schaper, J. Koch, F. Hohnsdorf, and W. Stolz, Cryst. Res. Technol. **35**, 787 (2000).
[58] S. R. Bank, M. A. Wistey, L. L. Goddard, H. B. Yuen, and J. S. Harris, Electron. Lett. **40**, 1186 (2004).
[59] M. A. Wistey, S. R. Bank, H. B. Yuen, and J. S. Harris Jr., J. Cryst. Growth **278**, (2005).
[60] H. B. Yuen, M. A. Wistey, S. R. Bank, H. P. Bae, and J. S. Harris Jr., J. Vac. Sci. Technol. B **23**, 1328 (2005).
[61] H. B. Yuen, S. R. Bank, M. A. Wistey, A. Moto, and J. S. Harris Jr., J. Appl. Phys. **96**, 6375 (2004).
[62] H. B. Yuen, S. R. Bank, M. A. Wistey, J. S. Harris Jr, M.-J. Seong, S. Yoon, R. Kudrawiec, and J. Misiewicz, J. Appl. Phys. **97**, 113510 (2005).
[63] K. Volz, V. Gambin, W. Ha, M. A. Wistey, H. B. Yuen, S. R. Bank, and J. S. Harris Jr., J. Cryst. Growth **251**, 360 (2003).
[64] S. R. Bank, H. P. Bae, H. B. Yuen, M. A. Wistey, L. L. Goddard, and J. S. Harris Jr., submitted to IEEE Photon. Technol. Lett.
[65] W. Ha, V. Gambin, M. Wistey, S. Bank, S. Kim, and J. S. Harris, IEEE Photon. Technol. Lett. **14**, 591 (2002).
[66] V. Gambin, W. Ha, M. Wistey, H. Yuen, S. R. Bank, S. M. Kim, and J. S. Harris, IEEE J. Sel. Top. Quantum Electron. **8**, 795 (2002).
[67] C. G. Van de Walle, Phys. Rev. B **39**, 1871 (1989).
[68] J. Misiewicz, R. Kudrawiec, K. Ryczko, G. Sęk, A. Forchel, J. C. Harmand, and M. Hammar, J. Phys.: Condens. Matter **16**, 3071 (2004).
[69] R. Kudrawiec, K. Ryczko, J. Misiewicz, H. B. Yuen, S. R. Bank, M. A. Wistey, H. P. Bae, and J. S. Harris Jr., Appl. Phys. Lett. **86**, 141908 (2005).
[70] R. Kudrawiec, M. Gladysiewicz, J. Misiewicz, H. B. Yuen, S. R. Bank, M. A. Wistey, H. P. Bae, and J. S. Harris Jr., Phys. Rev. B **73**, 245413 (2006).
[71] R. Kudrawiec, H. B. Yuen, M. Motyka, M. Gladysiewicz, J. Misiewicz, S. R. Bank, H. P. Bae, M. A. Wistey, and J. S. Harris, J. Appl. Phys. **100**, 013504 (2007).
[72] R. Kudrawiec, H. B. Yuen, K. Ryczko, J. Misiewicz, S. R. Bank, M. A. Wistey, H. P. Bae, and J. S. Harris Jr, J. Appl. Phys. **97**, 053515 (2005).
[73] W. Shan, W. Walukiewicz, J. W. Ager, III, E. E. Haller, J. F. Geisz, D. J. Friedman, J. M. Olson, and S. R. Kurtz, Phys. Rev. Lett. **82**, 1221 (1999).

[74] S. R. Bank, H. P. Bae, H. B. Yuen, M. A. Wistey, L. L. Goddard, J. S. Harris Jr., R. Kudrawiec, M. Gladysiewicz, M. Motyka, and J. Misiewicz, 25th Conference on Lasers and Electro Optics (CLEO), Long Beach, CA, USA, May 2006, Session CtuX6.
[75] R. Kudrawiec, S. R. Bank, H. P. Bae, H. B. Yuen, M. A. Wistey, L. L. Goddard, J. S. Harris Jr. M. Gladysiewicz, M. Motyka, and J. Misiewicz, Appl. Phys. Lett. **90**, 131905 (2007).
[76] P. J. Klar, H. Grüning, J. Koch, S. Schäfer, K. Volz, W. Stolz, W. Heimbrodt, A. M. Kamal Saadi, A. Lindsay, and E. P. O'Reilly, Phys. Rev. B **64**, 121203(R) (2001).
[77] V. Lordi, S. Friedrich, T. Funk, T. Takizawa, K. Uno, and J. S. Harris, Phys. Rev. Lett. **90**, 145505 (2003).
[78] R. Kudrawiec, G. Sek, J. Misiewicz, D. Gollub, and A. Forchel, Appl. Phys. Lett. **83**, 2772 (2003).
[79] R. Kudrawiec, E.-M. Pavelescu, J. Wagner, G. Sęk, J. Misiewicz, M. Dumitrescu, J. Konttinen, A. Gheorghiu, and M. Pessa, J. Appl. Phys. **96**, 2576 (2004).
[80] V. Lordi, H. B. Yuen, S. R. Bank, M. A. Wistey, J. S. Harris, and S. Friedrich, Phys. Rev. B **71**, 125309 (2005).
[81] R. Kudrawiec, G. Sęk, J. Misiewicz, L. H. Li, and J. C. Harmand, Eur. Phys. J. Appl. Phys. **27**, 313 (2004).
[82] M. Hugues, B. Damilano, J.-M Chauveau, J.-Y. Duboz, and J. Massies, Phys. Rev. B **75**, 045313 (2007).
[83] H. B. Yuen, S. R. Bank, H. Bae, M. A. Wistey, and J. S. Harris Jr., Appl. Phys. Lett. **88**, 221913 (2006).
[84] S. R. Bank, H. B. Yuen, M. A. Wistey, V. Lordi, H. P. Bae, and J. S. Harris Jr., Appl. Phys. Lett. **87**, 021908 (2006).
[85] S. R. Bank, H. B. Yuen, H. Bae, M. A. Wistey, A. Moto, and J. S. Harris Jr., Appl. Phys. Lett. **88**, 241923 (2006).
[86] S. R. Bank, H. B. Yuen, H. Bae, M. A. Wistey, and J. S. Harris Jr., Appl. Phys. Lett. **88**, 221115 (2006).
[87] I. A. Buyanova, W. M. Chen, G. Pozina, J. P. Bergman, B. Monemar, H. P. Xin, and C. W. Tu, Appl. Phys. Lett. **75**, 501 (1999).
[88] H. Y. Liu, C. M. Tey, C. Y. Jin, S. L. Liew, P. Navaretti, M. Hopkinson, and A. G. Cullis, Appl. Phys. Lett. **88**, 191907 (2006).
[89] S. R. Bank, H. Bae, H. B. Yuen, L. L. Goddard, M. A. Wistey, and J. S. Harris Jr., to be submitted to J. Cryst. Growth.
[90] H. Shimizu, K. Kumada, S. Uchiyama, and A. Kasukawa, Electron. Lett. **36**, 1701 (2000).
[91] S. R. Bank, H. P. Bae, H. B. Yuen, M. A. Wistey, L. L. Goddard, and J. S. Harris, Electron. Lett. **42**, 39 (2006).
[92] C. W. Coldren, M. C. Larson, S. G. Spruytte, and J. S. Harris, Electron. Lett. **36**, 951 (2000).
[93] M. C. Larson, C. W. Coldren, S. G. Spruytte, and J. S. Harris, IEEE Photonics Technol. Lett. **12**, 1598 (2000).
[94] J. S. Harris Jr., H. Yuen, M. Wistey, S. Bank, V. Lordi, T. Gugov, H. Bae, and L. Goddard, in: Dilute Nitride Semiconductors, edited by M. Henini (Elsevier, Amsterdam, 2005), Chapter 1 and references therein.
[95] M. A. Wistey, S. R. Bank, H. P. Bae, H. B. Yuen, E. R. Pickett, L. L. Goddard, and J. S. Harris, Electron. Lett. **42**, 282 (2006).
[96] S. R. Bank, H. P. Bae, H. B. Yuen, L. L. Goddard, M. A. Wistey, T. Sarmiento, and J. S. Harris, Optical Fiber Conference (OFC), Anaheim, CA (2006), paper OThN6.
[97] S. R. Bank, H. P. Bae, L. L. Goddard, H. B. Yuen, M. A. Wistey, and J. S. Harris, Device Research Conf., State College, PA (2006), paper II.A-7.
[98] N. Tansu, J. Y. Yeh, and L. J. Mawst, IEEE J. Sel. Top. Quantum Electron. **9**, 1220 (2003).
[99] N. Tansu, J. Y. Yeh, and L. J. Mawst, Appl. Phys. Lett. **83**, 2512 (2003).
[100] V. Lordi, H. B. Yuen, S. R. Bank, and J. S. Harris, Appl. Phys. Lett. **85**, 902 (2004).
[101] L. Du, J. C. Harmand, O. Mauguin, L. Largeau, L. Travers, and J. L. Oudar, Appl. Phys. Lett. **88**, 201110 (2006).
[102] D. J. Friedman, S. R. Kurtz, and J. F. Geisz, Conference Record of the Twenty-Ninth IEEE Photovoltaic Specialists Conference, New Orleans, LA, USA, May 2002, pp. 856–859.
[103] D. Jackrel et al., Proceedings of the 4th World Conference on Photovoltaic Energy Conversion, Hawai, USA, May 2006.
[104] D. R. Myers et al., Conference Record of the Twenty-Eighth IEEE Photovoltaic Specialists Conference, Anchorage, AK, USA, September 2000, p. 1202.
[105] S. Kurtz, A. Ptak, S. Bank, H. Yuen, M. Wistey, D. Friedman, S. Kurtz, and J. S. Harris, Jr., Conference Record of the Thirty-first IEEE Photovoltaic Specialists Conference, Orlando, USA, January 2005, pp. 707–710.

[106] A. J. Ptak, S. R. Kurtz, K. Emery, C. Whitaker, and T. Townsend, J. Appl. Phys. **98**, 094501 (2005).
[107] S. Kurtz, J. F. Geisz, D. J. Friedman, A. J. Ptak, R. R. King, D. C. Law, and N. H. Karam, Conference Record of the Twenty-eighth IEEE Photovoltaic Specialists Conference, Anchorage, AK, USA, September 2000, p. 1210.
[108] S. R. Kurtz, D. J. Friedman, S. Kurtz, and R. C. Reedy, Appl. Phys. Lett. **77**, 400 (2000).
[109] R. R. King, D. C. Law, C. M. Fetzer, R. A. Sherif, K. M. Edmondson, S. Kurtz, G. S. Kinsey, H. L. Cotal, D. D. Krut, J. H. Ermer, and N. H. Karam, Presented at the 20th European Photovoltaic Solar Energy Conference and Exhibition, Barcelona, Spain, June 2005.
[110] D. J. Friedman, J. M. Olson, S. Ward, T. Moriarty, K. Emery, S. Kurtz, A. Duda, R. R. King, H. L. Cotal, D. R. Lillington, J. H. Ermer, N. H. and N. H. Karam, Conference Record of the Twenty-Eighth IEEE Photovoltaic Specialists Conference, Anchorage, AK, USA, September 2000, pp. 965–967.
[111] A. A. Elemawy, H. J. Cao, E. Zhmayev, J. H. Lee, D. Zubia, and M. Osinski, phys. stat. sol. (b) **228**, 263 (2001).
[112] D. K. Shih, H. H. Lin, L. W. Sung, T. Y. Chu, and T. R. Yang, Jpn. J. Appl. Phys., Part 1 **42**, 375 (2003).
[113] T. D. Veal, I. Mahboob, and C. F. McConville, Phys. Rev. Lett. **92**, 136801 (2004).
[114] H. B. Yuen, Growth and characterization of dilute nitride antimonides for long-wavelength optoelectronics, Ph.D. thesis, Stanford University (2006).
[115] H. B. Yuen, S. M. Kim, F. Hatami, J. S. Harris, and A. H. Chin, Appl. Phys. Lett. **89**, 121912 (2006).

